Impact of Co-Fe Overlayers on Charge Carrier Dynamics at WO3/BiVO4 Heterojunctions: A Picosecond-to-Second Spectroscopic Analysis

Impact of Co-Fe Overlayers on Charge Carrier Dynamics at $WO_3/BiVO_4$ Heterojunctions: a Picosecond to Second Spectroscopic Analysis

Pierpaolo Vecchi[a,b], Federica Ruani[c], Michele Mazzanti[d], Quentin R. Loague[b], Raffaello Mazzaro[a,e*], Federico Boscherini[a], Barbara Ventura[c], Gerald J. Meyer[b*], Nicola Armaroli[c], Stefano Caramori[d], Luca Pasquini[a,e]

[a]*Department of Physics and Astronomy, University of Bologna, Viale Berti Pichat 6/2, 40127, Bologna, Italy*

[b]*Department of Chemistry, University of North Carolina at Chapel Hill, Chapel Hill, North Carolina 27599, USA.*

[c]*Istituto per la Sintesi Organica e la Fotoreattività (ISOF), Consiglio Nazionale delle Ricerche (CNR), Via P. Gobetti 101, Bologna 40129, Italy*

[d]*Department of Chemical, Pharmaceutical and Agricultural Sciences, University of Ferrara, Via Fossato di Mortara 17, 44121 Italy*

[e]*Istituto per la Microelettronica e Microsistemi (IMM), Consiglio Nazionale delle Ricerche (CNR), Via P. Gobetti 101, Bologna 40129, Italy*

*Corresponding authors: Raffaello Mazzaro | Email: raffaello.mazzaro@unibo.it
Gerald J. Meyer | Email: gjmeyer@unc.edu

Abstract

Surface modification with CoFe-based overlayers has been widely studied to improve the performance of $WO_3/BiVO_4$ photoanodes for photoelectrochemical water oxidation, because such overlayers can increase the photocurrent and shift the onset potential to more favorable values. Herein, we present a transient absorption spectroscopic analysis of $WO_3/BiVO_4$ photoanodes coated with cobalt iron oxide or cobalt iron Prussian blue overlayers, designed to establish the underlying mechanisms for these enhancements on the picosecond to second timescale. The data reveals that the overlayer suppresses recombination of trapped holes in $BiVO_4$, with free and trapped electrons, and accepts photogenerated holes. These results show that the observed boost in efficiency for water oxidation can be explained by the dual role of the overlayer in inhibiting charge recombination and enhancing charge extraction.

TOC Graphics

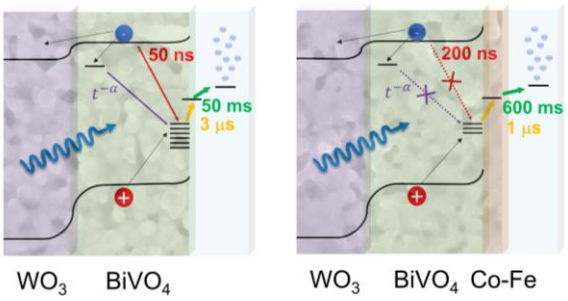

The quest for efficient and sustainable energy conversion has prompted intensive efforts to investigate photoelectrochemical (PEC) cells for water splitting, where the direct conversion of solar energy into clean hydrogen fuel is an attractive prospect.[1–3] Photoanodes are crucial for this purpose, since the rate determining step of the whole process is the oxygen evolution reaction.[4] Among the many semiconductors investigated as photoanodes, the heterojunction between tungsten trioxide (WO_3) and bismuth vanadate ($BiVO_4$) has emerged as a promising candidate due to its efficient light absorption across the UV-Vis spectral window, its ability to spatially separate charges leading to low carrier recombination, and its noteworthy photochemical selectivity for water oxidation.[5,6] In order to further enhance the photoanode performance, surface modification with cobalt-based overlayers has been intensively tested, in particular after the work of Nocera's group where cobalt phosphate (CoPi) emerged as an electrocatalyst for water oxidation in a neutral medium.[7] Since then, CoPi deposited on the surface of photoanodes has been widely studied for PEC water oxidation. However, CoPi's ability to collect photogenerated holes and catalyze water oxidation,[8,9] rather than only slowing down recombination by assisting in charge separation[10,11] remains contentious. Cobalt has also been integrated onto $BiVO_4$ surfaces in alternative forms, such as cobalt iron oxide ($CoFeO_x$)[12,13] or cobalt iron Prussian blue (CoFe-PB).[6,14] While the role of Fe is still a matter of debate[15,16], both afford significant enhancement in charge separation, leading to decreased surface recombination and improved overall efficiency. Understanding the charge carrier dynamics is crucial when designing such complex systems that need to efficiently separate charges across different interfaces.

Operando transient absorption spectroscopy (TAS) is a powerful tool to elucidate the intricate charge carrier dynamics and interfacial processes that govern the performance of PEC systems. The processes that limit the performance of the unmodified $WO_3/BiVO_4$ heterojunction and the beneficial effect of the two overlayers have been investigated on very different timescales and usually focus only on ultrafast (from ps to μs) electron-hole recombination[17–22] or on slow kinetics (from ms to s) where holes are transferred to the solution and the water oxidation reaction actively occurs[14,23–25]. In this work, we report the first TAS analysis of $WO_3/BiVO_4$ heterojunctions functionalized at the surface with $CoFeO_x$ and CoFe-PB. Moreover, this is the first kinetic study that characterizes the reaction dynamics from charge carrier generation (fs-ps) to the subsequent hole transfer reaction (ms) for PEC water splitting. Herein, we investigate the ultrafast electron-hole recombination processes and directly correlate them to the long-lived charge carriers useful for water oxidation, offering a unique perspective on the overall kinetics within the photoanode.

Our analysis and modelling provide a mechanistic description of the fate of photogenerated carriers with a relatively low number of kinetic processes, while monitoring the decay of the population of trapped holes in $BiVO_4$. These findings underscore the importance of multiscale analysis of TAS data to shed light on the interplay between charge carrier dynamics and surface processes within modified photoanodes, paving the way for the design of more efficient photoanode materials for sustainable energy conversion.

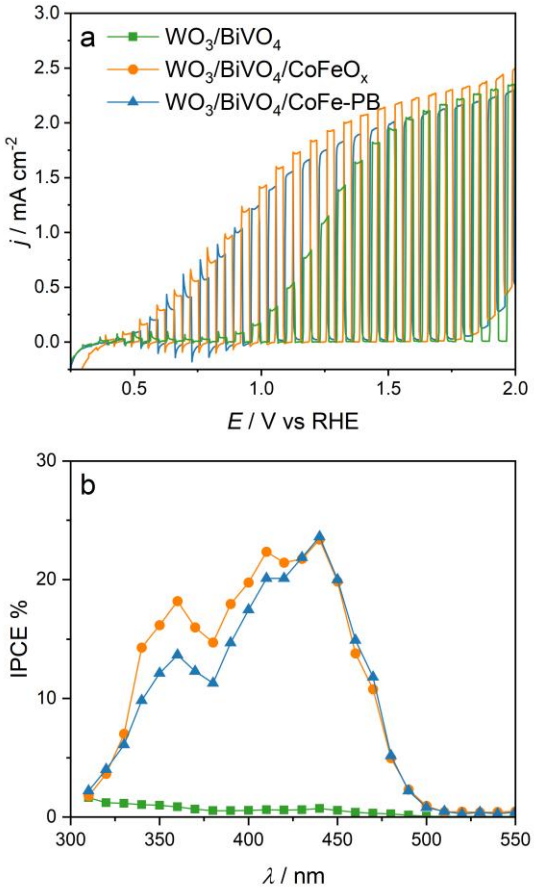

Figure 1: a) Chopped linear sweep voltammetry on the indicated samples. Scan rate 50 mV s^{-1}, AM 1.5G illumination from FTO side in phosphate buffer 0.1M. b) Incident photon-to-current conversion efficiency measurements at 0.8 V_{RHE}.

The bulk WO_3 layer was prepared via a sol-gel technique that afforded a colloidal structure, with the heterojunction formed by electrodeposition of $BiVO_4$. The two overlayers were deposited with different methods: $CoFeO_x$ through electrodeposition and CoFe-PB *via* surface ionic layer adsorption and reaction (SILAR). Complete description of the synthetic methods is available in the supporting information, together with morphological (Figure S1) and structural characterization by X-ray Absorption Spectroscopy (XAS, Figures S2-S3).

The deposition of Co-Fe overlayers resulted in an enhancement of the photoelectrochemical properties of $WO_3/BiVO_4$ heterojunctions. Figure 1a shows chopped linear sweep voltammetry measurements under AM 1.5G illumination, where the modified photoanodes exhibited a slight increase in photocurrent at the *plateau* and a remarkable shift of the photocurrent onset to more cathodic potentials. The incident photon-to-current conversion efficiency (IPCE) measurements

shown in Figure 1b were performed at low anodic bias (0.8 V_{RHE}) and show that the IPCE is about 20 times larger when overlayers of $CoFeO_x$ or CoFe-PB are deposited on the $WO_3/BiVO_4$.

Time-resolved spectral analysis. Figure 2 compares the ultrafast (10^{-12} s to 10^{-9} s range) TA spectra measured for the $WO_3/BiVO_4$ photoanodes with and without CoFe-based overlayers, in the absence of an applied bias (open circuit potential, OCP). TA spectra collected at various applied potentials are reported in Figure S5, displaying consistent spectral features. All TA spectra display three main features in the UV-Vis-NIR, in agreement with previous studies on $BiVO_4$ and $WO_3/BiVO_4$ photoanodes: i) a well-defined band centered at about 470 nm assigned to trapped holes in $BiVO_4$[26] due to transitions from the valence band (VB) into intraband gap (IBG) states emptied by ultrafast (≈ 1 ps) trapping of photoexcited holes;[17,19,27] ii) a broad band between 550 nm and 700 nm (partly convoluted with modulations due to thin-film interference) assigned to intraband transitions of free holes in the valence band;[17,19,27] and iii) a broad absorbance in the NIR region assigned to intraband transitions of free conduction band (CB) electrons.[28,29]

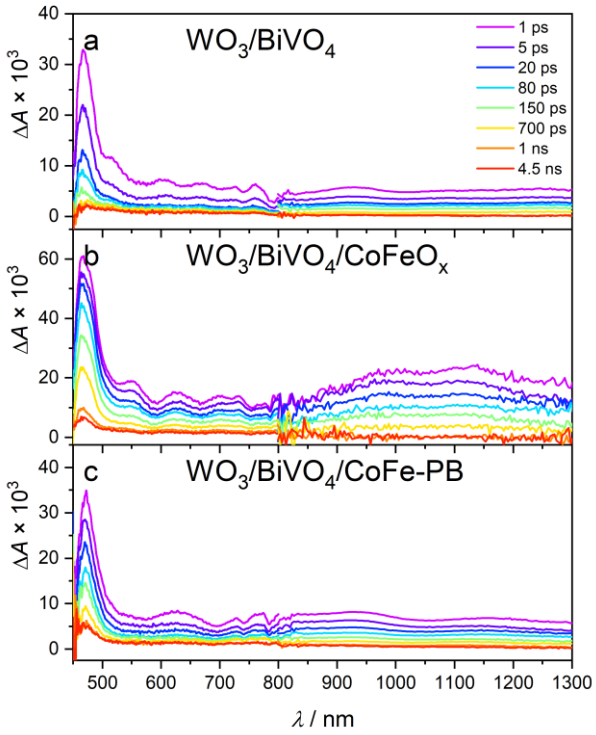

Figure 2: TA spectra measured after pulsed 430 nm excitation (100 fs, 5 μJ/pulse, 1mm^2 area) of a) $WO_3/BiVO_4$, b) $WO_3/BiVO_4/CoFeO_x$, and c) $WO_3/BiVO_4$/CoFe-PB at OCP in phosphate buffer 0.1M (pH 7) at the indicated time delays.

The same spectral features were observed until the ms range (Figure S6) for $WO_3/BiVO_4/CoFeO_x$ and $WO_3/BiVO_4$/CoFe-PB, while they gradually faded out for bare $WO_3/BiVO_4$. The decrease of the peak centered at 470 nm upon addition of Na_2SO_3 hole scavenger confirms its nature (Figure S7). In fact, surface trapped holes can be rapidly filled by the electron donor, leading to a significant drop of the 470 nm TA in the fast time scale, in agreement with previous reports.[22] Since these IBG states, responsible for hole trapping, are mainly located in proximity to the $BiVO_4$ surface and are known to represent a crucial step for water oxidation,[14,27] we focus the analysis on the main band at 470 nm by following its decay as a function of time. The TA kinetics at 0.8 V_{RHE} applied potential over three distinct time regimes are reported in Figures 3a (ps-ns), Figure 4a (ns–µs), and Figure 5a (ms–s). For each time domain, the best-fit parameters are summarized on the side of the kinetic traces (panels b-e). The dependence of TA kinetics on the applied potential are summarized in Figure S8 on a double logarithmic scale to encompass the full ps-s time interval. Here, the amplitude discontinuity from the ps–ns to the ns–µs regime is due to the different fluence of the excitation source, which is about 10 times lower in the ps-ns range (see also SI, figure S4).

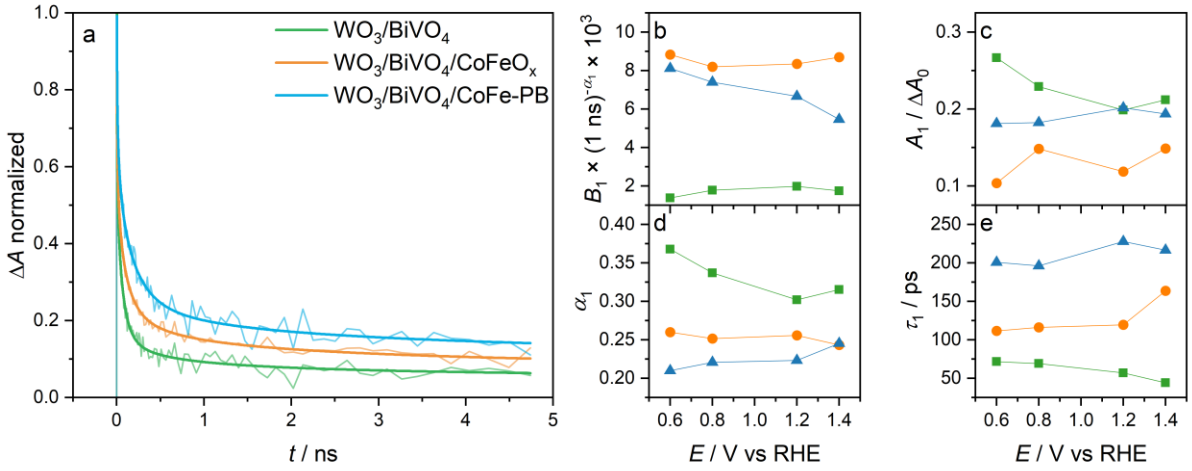

Figure 3: a) TA kinetics monitored at 470 nm on the ps to ns domain, upon 430 nm excitation (100 fs, 0.5 mJ/cm^2 pulses, 1 mm^2 area) of the indicated materials normalized at 1 ps (0.8 V_{RHE} in phosphate buffer 0.1M, pH 7). Overlaid thick lines are fits to Equation 1. The best fit parameters for non-normalized kinetics are reported in b-e) as a function of the applied potential, respectively power law amplitude after 1 ns delay (b) and exponent α_1 (d), as well as exponential amplitude (c) and time constant τ_1 (e).

Picosecond-to-nanosecond timescale. Figure 3a shows an overall stronger persistence of the 470 nm trapped holes signal in the presence of overlayers, in comparison with bare $WO_3/BiVO_4$. The linear trend visible at $\approx 2-50$ ps in the log-log plot (Figure S8a,d,g) suggests that the initial

decay follows a power law, while an additional decay develops at longer times; therefore, the TA kinetics were fit according to Equation 1:

$$\Delta A(t) = B_1 t^{-\alpha_1} + A_1 \exp\left(-\frac{t}{\tau_1}\right) \quad (1)$$

Since the following discussion deeply correlates to the employed fitting model, it must be noted that other viable models are available to fit the transient response of analogous systems, such as the combination of power law and stretched exponential[30], or multiexponential fittings[22]. A representative comparison between the goodness of fit of the proposed model[25] and several options reported in literature is reported in the SI (Figure S9). Equation 1 yields similar statistics to a triple exponential model but uses significantly less parameters (4 vs 7), and performs much better than the other models. Furthermore, it is directly applicable also to the extended time domain, as discussed later on, thus allowing for a coherent interpretation of the experimental data.

Physically, the power law represents diffusion-limited recombination processes involving localized carriers,[31,32] which undergo relaxation within a broadened density of states.[19,33] Therefore, it is reasonable to assign the power law decay to the non-ideal second-order recombination of holes trapped at IBG states with shallowly trapped electrons. This dispersive process occurs at all time scales and corresponds to the sum of exponential functions with a distribution of characteristic times.[34] We depicted this using purple arrows in Scheme 1, which summarizes graphically the charge recombination and transfer steps inferred from TAS. The exponent α_1 is significantly reduced by the addition of $CoFeO_x$ and CoFe-PB overlayers. It ranged from $0.37 - 0.30$ in the bare photoanode, down to $0.26 - 0.21$, whereas the applied bias has a small and non-monotonous effect (Figure 3b). Typical values of the power law exponent in the literature are in the range $0.2 - 0.5$, in good agreement with these ps results and those in the extended ns - s range (*vide infra*).[19,27,32] Since smaller α_1 values are associated with longer-lived transient signals (Figure S10), we infer that the overlayers significantly reduce the dispersive recombination of trapped holes. In addition, the power law exponent can be correlated to the energy distribution of the traps; for instance, the average energy E_0 of an exponential tail above the VB obeys the relation $E_0 = k_b T/\alpha$.[35,36] Microscopically, this suggests that the overlayers shift the average energy of IBG states slightly upward, making it more difficult for the holes to undergo thermally activated detrapping and recombination.

The exponential decay with a characteristic time τ_1 describes a first-order kinetic process that has been previously assigned to recombination of trapped holes with free electrons in the CB,[17–19] as illustrated by the red arrows in Scheme 1. In support of this interpretation, a similar exponential decay with amplitude $A_1^{el} \approx 0.8$ mOD and time $\tau_1^{el} \approx 70$ ps was extracted from the kinetic data measured for the bare photoanode at 1000 nm, which is representative of free electrons (Figure S11). The magnitude of both A_1 and A_1^{el} strongly decreases with the addition of overlayers, especially with $CoFeO_x$, due to reduced probability of recombination for this specific pathway. Consistently, the lifetime τ_1 (Figure 3e) increased with overlayer addition, from $50 - 70$ ps in the uncoated sample to $100 - 150$ and $200 - 250$ ps in the samples with $CoFeO_x$ and CoFe-PB, respectively. Therefore, first-order recombination of trapped holes with CB electrons is hindered after addition of $CoFeO_x$ and CoFe-PB overlayers. This observation as well as the decrease of α_1 can be explained by the overlayer-induced passivation of surface IBG states, which leads to Fermi level unpinning.[37] In order to provide further evidence in this direction, we have performed electrochemical impedance spectroscopy in the dark (EIS) and under illumination (PEIS), as described in the SI. Figure S13 shows that the overlayers induce both a significant decrease of the chemical capacitance associated with surface states and a cathodic shift of their distribution, the latter being consistent with the decrease of the power-law exponent in presence of overlayers (*vide supra*). The removal of surface IBG states is expected to enhance band bending in the space charge region, facilitating photoexcited charge separation and leading to an anticipated photocurrent onset in the J/V curves.

Nanosecond-to-millisecond timescale. The 10 ns – 0.1 ms TA kinetics are reported in Figures 4a and S8b,e,h. Here, the linear trend in the log-log plot highlights again the presence of an underlying power law decay; in addition, with increasing applied potential, an exponential decay with characteristic time of 1-3 µs becomes more relevant. Accordingly, the kinetic data were fit to the sum of a power law and an exponential decay:

$$\Delta A(t) = B_2 t^{-\alpha_2} + A_2 \exp\left(-\frac{t}{\tau_2}\right) \quad (2)$$

Note that Equation 2 has the same functional form of Equation 1. By this time, the electrons photoexcited in the CB either recombined with holes or are trapped. Indeed, Ravensbergen *et al*. have identified a characteristic time of 2.5 ns for electronic transition into shallow traps of $BiVO_4$.[19]

Since the first-order recombination time is short $\tau_1 \ll 1$ ns (*vide supra*), only the dispersive recombination channel remains active. The α_2 values reported in Figure 4c are close to 0.5, in excellent agreement with the value of 0.49 reported by Ravensbergen *et al*. in a similar time window.[19] The increase of α_2 compared to α_1 is mainly due to the 10x higher laser fluence, which heavily affects the power law exponent.[27] This is demonstrated by the comparison reported in Figure S12 between TA kinetics recorded on bare $WO_3/BiVO_4$ after pumping with fluences of 5 mJ/cm^2 and 0.5 mJ/cm^2; a decrease from $\alpha_2 \approx 0.50$ down to $\alpha_2 \approx 0.29$ is observed, the latter value being very close to $\alpha_1 \approx 0.34$ measured at the same fluence in the ps-ns range. A slight decrease with increasing time was expected because the average energy of filled traps shifts to deeper values as the shallower traps are depopulated.

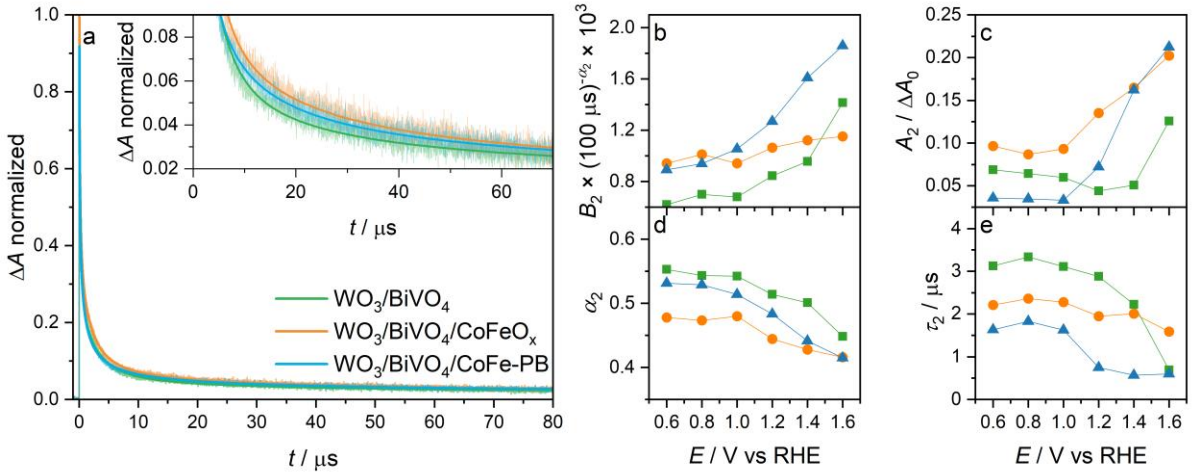

Figure 4: a) TA kinetics monitored at 470 nm in the 10 ns to 0.1 ms domain, upon 355 nm excitation (6 ns, 5 mJ/cm^2 pulses, 1 cm^2 area) of the indicated samples. The data was normalized at 40 ns (0.8 V_{RHE} in phosphate buffer 0.1M, pH 7). Overlaid thick lines are fits to Equation 2. Best fit parameters for non-normalized data are reported in b-e) as a function of the applied potential, respectively power law amplitude after 100 µs delay (b) and exponent α_2 (d), as well as exponential amplitude (c) and time constant τ_2 (e).

We notice that α_2 decreases slightly with increasing applied potential and by the addition of the overlayers (especially $CoFeO_x$, Figure 4d); this translates into a higher density of trapped holes that have survived recombination at a given time t^*, as shown in Figure 4b by the value $B_2 \cdot (t^*)^{-\alpha_2}$ (proportional to the trapped hole density) for $t^* = 100$ µs. The same conclusion can be clearly drawn by comparison with the 100 µs TA spectra in Figure S6. Therefore, it appears that the overlayers produce an effect similar to the applied potential in promoting the separation of free

or shallowly trapped electrons from the trapped holes. This observation corroborates the idea that the overlayers enhance the built-in electric field via defect passivation and Fermi level unpinning.

An important difference between the ps and ns regimes emerges when examining the behavior of the exponential component (Figure 4c): the characteristic time τ_2 at $0.6 - 1.0$ V_{RHE} drops significantly from ≈ 3 µs for the uncoated photoanode down to $2.0 - 1.5$ µs when an overlayer was deposited (rather than increasing as τ_1) and a further decrease is observed with more anodic applied potentials. Furthermore, the A_2 amplitude rises significantly with increased potential above 1.0 V_{RHE}. Therefore, this component describes a depopulation of trapped holes, which is enhanced by both the overlayers and the potential, showing the same trend as the photocurrent displayed in Figure 1. This similarity clearly indicates that this kinetic process is not representative of charge losses due to recombination, but rather of the transfer of trapped holes towards intermediate charge transfer (CT) states, from which water oxidation and Faradaic photocurrent occurs. We remark that such intermediate transfer on a few µs scale, which is beneficial to the photoelectrochemical performance, was not directly identified in previous ultrafast studies.[19,21] Clearly, this characteristic time cannot be associated with direct injection into the electrolyte, which is known to occur on a much longer timescale (*vide infra*). The intermediate CT state can be associated with oxidized species adsorbed in proximity of surface oxygen vacancies in $BiVO_4$,[38–40] as well as with oxidized metal centers in the overlayer.[14] While Moss *et al*. reported complete hole transfer from $BiVO_4$ IBG traps to CoFe-PB overlayer in this time regime,[14] the lack of a specific spectral feature at about 700 nm in our TA spectra and the presence of the CT process on pristine WO_3/$BiVO_4$ leaves both hypotheses open. However, regardless of the species involved, the improved kinetics towards this intermediate CT state, with the addition of the overlayer, competes with the underlying power law recombination, thus enhancing charge separation. The intermediate CT state is depicted just outside the $BiVO_4$ layer in Scheme 1 and the transfer of trapped holes active at 470 nm is represented by the yellow arrows, that become thicker with applied potential and overlayer addition. Since the two competing recombination and CT channels show opposite dependencies on the presence of overlayers, the normalized kinetics of the bare photoanode display only a slightly slower decay compared to those of the coated ones, as shown by the inset of Figure 4a. This contrasts with the empirical observation in the ps-ns regime, where both recombinative channels are suppressed by the overlayers, resulting in a slower decay and higher final ΔA value.

Millisecond-to-second timescale. We choose to analyze the TA kinetics collected from 1 ms to 1 s (Figures 5a and S8c,f,i) using the sum of a power law and a single stretched exponential (Kohlrausch–Williams–Watts or KWW function) with $\beta = 0.5$ as a fit function, according to:

$$\Delta A(t) = B_2 t^{-\alpha_2} + A_3 \exp[-(t/\tau_3)^{\beta}] \quad (3)$$

where the parameters of the power-law decay have been fixed to those obtained in the previous case (for every sample and potential value). This approach implicitly assumes that the electron-hole recombination, described by the power law, is the same in the two different time windows, which is reasonable since the intensity and excitation wavelength are the same and the populations of trapped carriers relax slowly at this stage. The KWW decay describes hole injection into the electrolyte, leading to water oxidation with the typical characteristic time of tens to hundreds ms (Figure 5b and green arrow in Scheme 1).[41,42] This assignment is corroborated by the increased amplitude A_3 with the applied potential (Figure 5b), i.e., in the same range where the photocurrent rises significantly (Figure 1), with a particularly strong slope in the case of the $CoFeO_x$ overlayer.

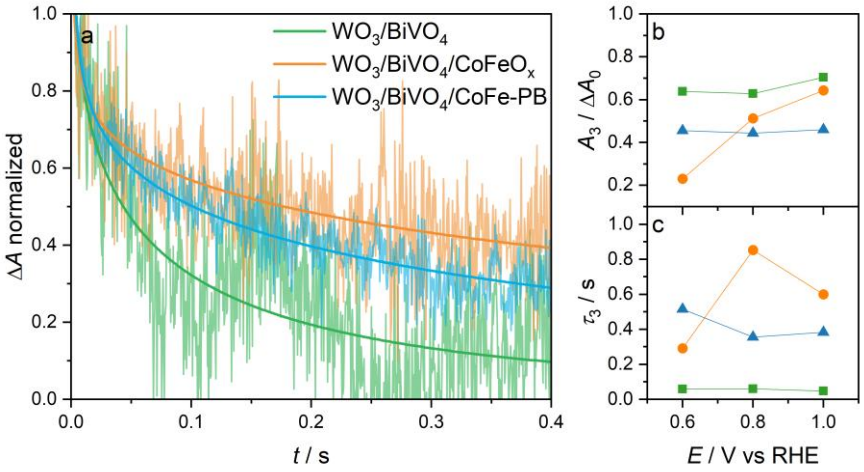

Figure 5: a) TA kinetics monitored at 470 nm on the ms to s time domain, upon 355 nm excitation (6 ns, 5 mJ/cm^2 pulses, 1 cm^2 area) normalized at 2 ms (0.8 V_{RHE} in phosphate buffer 0.1 M, pH 7). Overlaid thick lines are fits to Equation 3. Since power law parameters are fixed to the ones reported in Figure 4, only the exponential amplitude (b) and time constant τ_3 (c) are displayed.

We remark that TAS is not able to distinguish between hole transfer directly from the IBG states and *via* intermediate CT states. In fact, CT states do not contribute to absorption change at 470 nm, but the transfer of a hole from a CT state to the electrolyte (on a several ms scale) can be rapidly followed by hole transfer from IBG states into CT states on a μs time scale (yellow arrow

in Scheme 1), which is eventually detected as a decay in the absorption at 470 nm. In other words, the kinetics of hole injection via intermediate CT states contributes to the decay of the trapped holes through fast transfer between IBG and CT states. Overall, the KWW components describes a distribution of different hole injection pathways, i.e., direct and via CT states, which explains the need for a stretched rather than a simple exponential.

Interestingly, we notice that the overlayers extend the characteristic time τ_3 from 47 ms for $WO_3/BiVO_4$ to 380 ms with CoFe-PB and 600 ms with $CoFeO_x$ at 1 V_{RHE}. Since the overlayers have a beneficial impact on the photocurrent, especially in the 0.6 – 1.0 V_{RHE} range, the increased lifetime cannot reflect a slower injection into the electrolyte that would reduce the water oxidation rate. In order to understand this result, we point out that $\tau_3 = (k_{rec} + k_{tr})^{-1}$, where k_{rec} and k_{tr} are the rate constants for recombination and transfer.[14,27] Therefore, the increased lifetime can be ascribed to a decrease of k_{rec}. A similar explanation in terms of reduced recombination was also proposed by Ma *et al*. to interpret the lifetime increase with increasing V_{RHE} in photoanodes where k_{tr} is potential-independent.[25] Furthermore, this view is fully supported by a recent investigation carried out in our group using Intensity-Modulated Photocurrent Spectroscopy (IMPS),[6] which revealed that the CoFe-PB overlayer reduces k_{rec} compared to the bare photoanode, while k_{tr} remains unchanged.

Interestingly, no major difference is observed between CoFe-PB and $CoFeO_x$, suggesting that similar kinetics may result from *in situ* structural surface reconstruction under PEC operating conditions. XAS at Co K-edge was performed after the TAS characterization to shed light on this point. While X-ray fluorescence (Figure S14) shows an almost constant intensity, suggesting good stability of the overlayer amount on the surface, XAS (Figure S15) reveals a significant alteration after the TAS characterization. Remarkably, both the XANES and EXAFS of $CoFeO_x$ and CoFe-PB become very similar to those reported for neutral pH operating CoPi, credited to cluster-size CoO_6 octahedra bridged by oxo/hydroxo ligands[43] due to hydrous surface. This suggests that the overlayers attain a similar structure upon operation, independently on their initial state. Similar reconstruction processes were previously highlighted on Co-based catalysts, leading to pH-dependent structural features.[44]

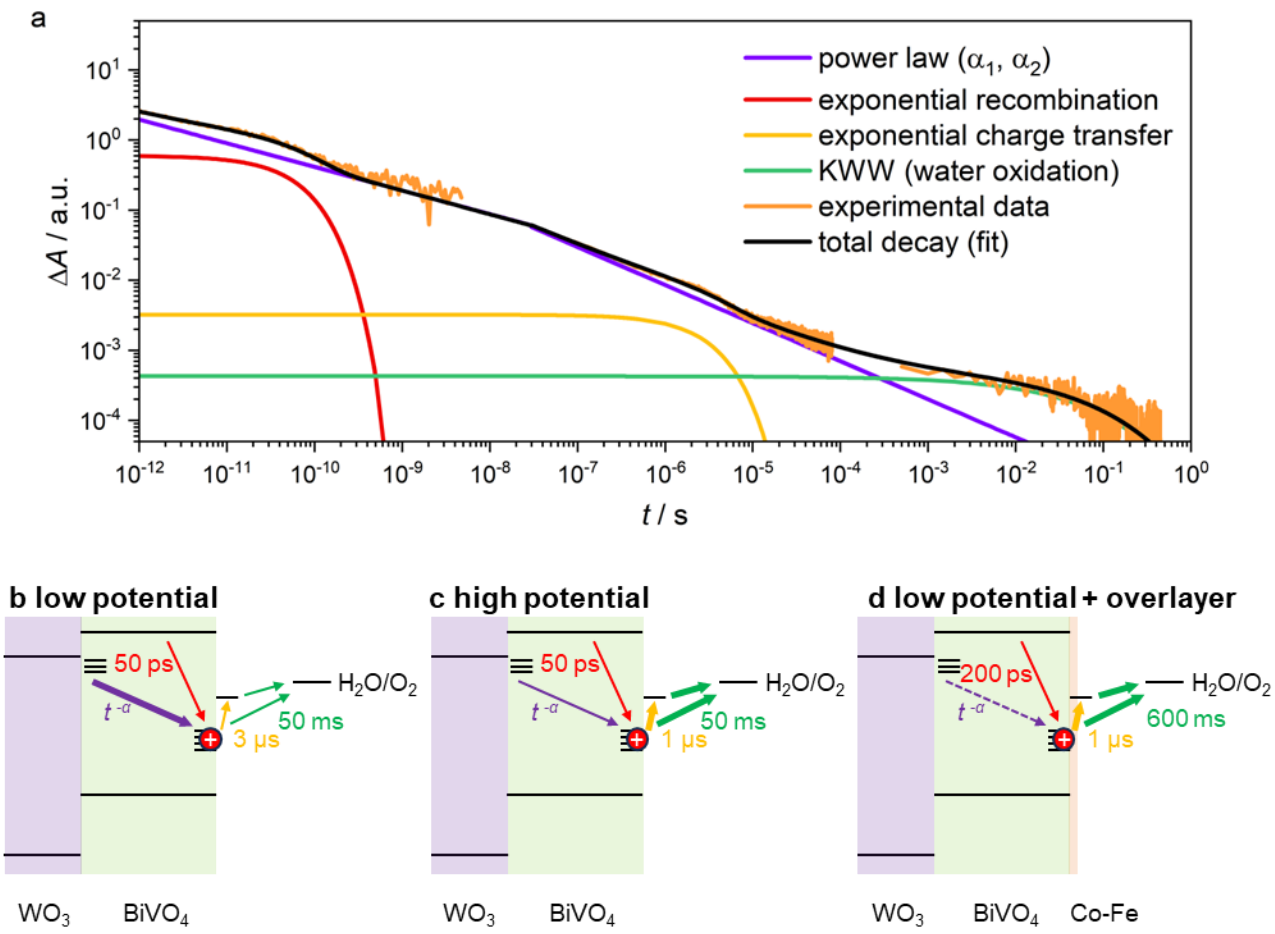

Scheme 1: a) TA kinetics from 1 ps to 1 s overlaid by relative fits. Band diagram showing the relevant detrapping processes under different conditions for b) $WO_3/BiVO_4$, c) $WO_3/BiVO_4$ at higher potential, and d) $WO_3/BiVO_4$ with Co-Fe overlayer at low potential. Dashed arrows and thicker arrows represent a decrease and an increase in amplitude, respectively. In a), ultrafast ΔA data have been scaled to provide continuity with those in the ns range. See text for a detailed explanation.

In conclusion, transient data measured over a time window spanning across twelve orders of magnitude were fit by simple kinetic models, which require a small number of processes with few fitting parameters and are able to provide a physical interpretation of photoexcited charge carrier dynamics. Building upon prior knowledge garnered by previous pump-probe studies, valuable understanding regarding the impact of CoFe-based overlayers on $WO_3/BiVO_4$ photoanodes were acquired, as outlined below:

- Decrease of the power-law recombination rate on all timescales, as well as the exponential recombination in the ps range, due to overlayer-induced passivation of surface states, possibly leading to Fermi level unpinning, enhanced built-in electric field, and overall improved charge separation efficiency;
- Overlayer-boosted transfer of holes on the ≈ 1 μs timescale from intra bandgap traps at the $BiVO_4$ surface to intermediate states, likely associated with oxidized sites in the overlayer, from which charge transfer into the electrolyte can take place on longer times;
- Increased lifetime of the KWW decay, associated with water oxidation in the tens to hundreds of ms timescale, indicating that the overlayers boost the photoelectrochemical performance by collecting holes and suppressing surface recombination, rather than by accelerating water oxidation kinetics.

Supporting Information

Experimental methods, structural characterization (SEM, XAS) of the samples before and after the TAS experiments, EIS characterization and additional TAS data.

Acknowledgements

This project has received funding from the European Union's Horizon 2020 research and innovation programme, under Grant Agreement No 101006839 (H2020 Research Innovation Actions 2020-2024 "CONDOR"). BV, FB, and NA gratefully acknowledge support from the EU community – Next Generation EU, under National Recovery and Resilience Plan (NRRP) project NEST-Network 4 Energy Sustainable Transition (PE0000021). The UNC-CH authors gratefully acknowledge support from the Division of Chemical Sciences, Office of Basic Energy Sciences, Office of Energy Research, US Department of Energy (DE-SC0013461).

References

(1) Lewis, N. S.; Nocera, D. G. Powering the Planet: Chemical Challenges in Solar Energy Utilization. *Proc Natl Acad Sci U S A* **2006**, *103* (43), 15729–15735. https://doi.org/10.1073/PNAS.0603395103.

(2) Listorti, A.; Durrant, J.; Barber, J. Artificial Photosynthesis: Solar to Fuel. *Nat Mater* **2009**, *8* (12), 929–930. https://doi.org/10.1038/nmat2578.

(3) Gust, D.; A. Moore, T.; L. Moore, A. Solar Fuels via Artificial Photosynthesis. *Acc Chem Res* **2009**, *42* (12), 1890–1898. https://doi.org/10.1021/ar900209b.

(4) Fabbri, E.; Habereder, A.; Waltar, K.; Kötz, R.; Schmidt, T. J. Developments and Perspectives of Oxide-Based Catalysts for the Oxygen Evolution Reaction. *Catal Sci Technol* **2014**, *4* (11), 3800–3821. https://doi.org/10.1039/C4CY00669K.

(5) Hong, S. J.; Lee, S.; Jang, J. S.; Lee, J. S. Heterojunction BiVO4/WO3 Electrodes for Enhanced Photoactivity of Water Oxidation. *Energy Environ Sci* **2011**, *4* (5), 1781–1787. https://doi.org/10.1039/C0EE00743A.

(6) Vecchi, P.; Piccioni, A.; Mazzaro, R.; Mazzanti, M.; Cristino, V.; Caramori, S.; Pasquini, L. Charge Separation Efficiency in WO_3 /$BiVO_4$ Photoanodes with CoFe Prussian Blue Catalyst Studied by Wavelength-Dependent Intensity-Modulated Photocurrent Spectroscopy. *Solar RRL* **2022**, 2200108. https://doi.org/10.1002/SOLR.202200108.

(7) Kanan, M. W.; Nocera, D. G. In Situ Formation of an Oxygen-Evolving Catalyst in Neutral Water Containing Phosphate and Co2+. *Science (1979)* **2008**, *321* (5892), 1072–1075. https://doi.org/10.1126/SCIENCE.1162018.

(8) Nellist, M. R.; Laskowski, F. A. L.; Qiu, J.; Hajibabaei, H.; Sivula, K.; Hamann, T. W.; Boettcher, S. W. Potential-Sensing Electrochemical Atomic Force Microscopy for in Operando Analysis of Water-Splitting Catalysts and Interfaces. *Nat Energy* **2018**, *3* (1), 46–52. https://doi.org/10.1038/S41560-017-0048-1.

(9) Nellist, M. R.; Qiu, J.; Laskowski, F. A. L.; Toma, F. M.; Boettcher, S. W. Potential-Sensing Electrochemical AFM Shows CoPi as a Hole Collector and Oxygen Evolution Catalyst on BiVO4 Water-Splitting Photoanodes. *ACS Energy Lett* **2018**, *3* (9), 2286–2291. https://doi.org/10.1021/acsenergylett.8b01150.

(10) Ma, Y.; Kafizas, A.; Pendlebury, S. R.; Le Formal, F.; Durrant, J. R. Photoinduced Absorption Spectroscopy of CoPi on BiVO4: The Function of CoPi during Water Oxidation. *Adv Funct Mater* **2016**, *26* (27), 4951–4960. https://doi.org/10.1002/ADFM.201600711.

(11) Zachäus, C.; Abdi, F. F.; Peter, L. M.; Van De Krol, R. Photocurrent of BiVO4 Is Limited by Surface Recombination, Not Surface Catalysis. *Chem Sci* **2017**, *8* (5), 3712–3719. https://doi.org/10.1039/c7sc00363c.

(12) Wang, S.; He, T.; Yun, J.-H.; Hu, Y.; Xiao, M.; Du, A.; Wang, L.; Wang, S.; Yun, J.; Hu, Y.; Xiao, M.; Wang, L.; He, T.; Du, A. New Iron-Cobalt Oxide Catalysts Promoting BiVO4 Films for

Photoelectrochemical Water Splitting. *Adv Funct Mater* **2018**, *28* (34), 1802685. https://doi.org/10.1002/ADFM.201802685.

(13) Lin, J.; Han, X.; Liu, S.; Lv, Y.; Li, X.; Zhao, Y.; Li, Y.; Wang, L.; Zhu, S. Nitrogen-Doped Cobalt-Iron Oxide Cocatalyst Boosting Photoelectrochemical Water Splitting of BiVO4 Photoanodes. *Appl Catal B* **2023**, *320*, 121947. https://doi.org/10.1016/J.APCATB.2022.121947.

(14) Moss, B.; Hegner, F. S.; Corby, S.; Selim, S.; Francàs, L.; López, N.; Giménez, S.; Galán-Mascarós, J.-R.; Durrant, J. R. Unraveling Charge Transfer in CoFe Prussian Blue Modified BiVO4 Photoanodes. *ACS Energy Lett* **2019**, *4* (1), 337–342. https://doi.org/10.1021/acsenergylett.8b02225.

(15) Li, N.; Hadt, R. G.; Hayes, D.; Chen, L. X.; Nocera, D. G. Detection of High-Valent Iron Species in Alloyed Oxidic Cobaltates for Catalysing the Oxygen Evolution Reaction. *Nat Commun* **2021**, *12* (1), 6–11. https://doi.org/10.1038/s41467-021-24453-6.

(16) Enman, L. J.; Stevens, M. B.; Dahan, M. H.; Nellist, M. R.; Toroker, M. C.; Boettcher, S. W. Operando X-Ray Absorption Spectroscopy Shows Iron Oxidation Is Concurrent with Oxygen Evolution in Cobalt–Iron (Oxy)Hydroxide Electrocatalysts. *Angewandte Chemie International Edition* **2018**, *57* (39), 12840–12844. https://doi.org/10.1002/anie.201808818.

(17) Grigioni, I.; Ganzer, L.; V. A. Camargo, F.; Bozzini, B.; Cerullo, G.; Selli, E. In Operando Photoelectrochemical Femtosecond Transient Absorption Spectroscopy of WO3/BiVO4 Heterojunctions. *ACS Energy Lett* **2019**, *4* (9), 2213–2219. https://doi.org/10.1021/acsenergylett.9b01150.

(18) Grigioni, I.; Stamplecoskie, K. G.; Jara, D. H.; Dozzi, M. V.; Oriana, A.; Cerullo, G.; Kamat, P. V.; Selli, E. Wavelength-Dependent Ultrafast Charge Carrier Separation in the WO3/BiVO4 Coupled System. *ACS Energy Lett* **2017**, *2* (6), 1362–1367. https://doi.org/10.1021/acsenergylett.7b00216.

(19) Ravensbergen, J.; Abdi, F. F.; Van Santen, J. H.; Frese, R. N.; Dam, B.; Van De Krol, R.; Kennis, J. T. M. Unraveling the Carrier Dynamics of BiVO4: A Femtosecond to Microsecond Transient Absorption Study. *Journal of Physical Chemistry C* **2014**, *118* (48), 27793–27800. https://doi.org/10.1021/jp509930s.

(20) Grigioni, I.; Polo, A.; Dozzi, M. V.; Stamplecoskie, K. G.; Jara, D. H.; Kamat, P. V.; Selli, E. Enhanced Charge Carrier Separation in WO3/BiVO4Photoanodes Achieved via Light Absorption in the BiVO4Layer. *ACS Appl Energy Mater* **2022**, *5* (11), 13142–13148. https://doi.org/10.1021/acsaem.2c02597.

(21) Prasad, U.; Young, J. L.; Johnson, J. C.; McGott, D. L.; Gu, H.; Garfunkel, E.; Kannan, A. M. Enhancing Interfacial Charge Transfer in a WO3/BiVO4 Photoanode Heterojunction through Gallium and Tungsten Co-Doping and a Sulfur Modified Bi2O3 Interfacial Layer. *J Mater Chem A Mater* **2021**, *9* (29), 16137–16149. https://doi.org/10.1039/d1ta03786b.

(22) Grigioni, I.; Stamplecoskie, K. G.; Selli, E.; Kamat, P. V. Dynamics of Photogenerated Charge Carriers in WO3/BiVO4 Heterojunction Photoanodes. *Journal of Physical Chemistry C* **2015**, *119* (36), 20792–20800. https://doi.org/10.1021/acs.jpcc.5b05128.

(23) Selim, S.; Francàs, L.; García-Tecedor, M.; Corby, S.; Blackman, C.; Gimenez, S.; Durrant, J. R.; Kafizas, A. WO3/BiVO4: Impact of Charge Separation at the Timescale of Water Oxidation. *Chem Sci* **2019**, *10* (9), 2643–2652. https://doi.org/10.1039/C8SC04679D.

(24) Cowan, A. J.; Durrant, J. R. Long-Lived Charge Separated States in Nanostructured Semiconductor Photoelectrodes for the Production of Solar Fuels. *Chem Soc Rev* **2013**, *42* (6), 2281–2293. https://doi.org/10.1039/c2cs35305a.

(25) Ma, Y.; Pendlebury, S. R.; Reynal, A.; Le Formal, F.; Durrant, J. R. Dynamics of Photogenerated Holes in Undoped BiVO4 Photoanodes for Solar Water Oxidation. *Chem Sci* **2014**, *5* (8), 2964–2973. https://doi.org/10.1039/c4sc00469h.

(26) Aiga, N.; Jia, Q.; Watanabe, K.; Kudo, A.; Sugimoto, T.; Matsumoto, Y. Electron-Phonon Coupling Dynamics at Oxygen Evolution Sites of Visible-Light-Driven Photocatalyst: Bismuth Vanadate. *Journal of Physical Chemistry C* **2013**, *117* (19), 9881–9886. https://doi.org/10.1021/jp4013027.

(27) Ma, Y.; Pendlebury, S. R.; Reynal, A.; Le Formal, F.; Durrant, J. R. Dynamics of Photogenerated Holes in Undoped BiVO4 Photoanodes for Solar Water Oxidation. *Chem Sci* **2014**, *5* (8), 2964–2973. https://doi.org/10.1039/c4sc00469h.

(28) M. Pesci, F.; J. Cowan, A.; D. Alexander, B.; R. Durrant, J.; R. Klug, D. Charge Carrier Dynamics on Mesoporous WO3 during Water Splitting. *J Phys Chem Lett* **2011**, *2* (15), 1900–1903. https://doi.org/10.1021/jz200839n.

(29) Corby, S.; Francàs, L.; Selim, S.; Sachs, M.; Blackman, C.; Kafizas, A.; Durrant, J. R. Water Oxidation and Electron Extraction Kinetics in Nanostructured Tungsten Trioxide Photoanodes. *J Am Chem Soc* **2018**, *140* (47), 16168–16177. https://doi.org/10.1021/jacs.8b08852.

(30) Cowan, A. J.; Tang, J.; Leng, W.; Durrant, J. R.; Klug, D. R. Water Splitting by Nanocrystalline TiO 2 in a Complete Photoelectrochemical Cell Exhibits Efficiencies Limited by Charge Recombination. *Journal of Physical Chemistry C* **2010**, *114* (9), 4208–4214. https://doi.org/10.1021/jp909993w.

(31) Toussaint, D.; Wilczek, F. Particle–Antiparticle Annihilation in Diffusive Motion. *J Chem Phys* **1983**, *78* (5), 2642–2647. https://doi.org/10.1063/1.445022.

(32) Nelson, J.; Haque, S. A.; Klug, D. R.; Durrant, J. R. Trap-Limited Recombination in Dye-Sensitized Nanocrystalline Metal Oxide Electrodes. *Phys Rev B* **2001**, *63* (20). https://doi.org/10.1103/PhysRevB.63.205321.

(33) Montanari, I.; Nogueira, A. F.; Nelson, J.; Durrant, J. R.; Winder, C.; Loi, M. A.; Sariciftci, N. S.; Brabec, C. Transient Optical Studies of Charge Recombination Dynamics in a Polymer/Fullerene Composite at Room Temperature. *Appl Phys Lett* **2002**, *81* (16), 3001–3003. https://doi.org/10.1063/1.1512943.

(34) Bochud, T.; Challet, D. Optimal Approximations of Power Laws with Exponentials: Application to Volatility Models with Long Memory. *Quant Finance* **2007**, *7* (6), 585–589. https://doi.org/10.1080/14697680701278291.

(35) Nelson, J. Diffusion-Limited Recombination in Polymer-Fullerene Blends and Its Influence on Photocurrent Collection. *Phys Rev B* **2003**, *67* (15). https://doi.org/10.1103/PhysRevB.67.155209.

(36) Godin, R.; Hisatomi, T.; Domen, K.; Durrant, J. R. Understanding the Visible-Light Photocatalytic Activity of GaN:ZnO Solid Solution: The Role of Rh2−yCryO3 Cocatalyst and Charge Carrier Lifetimes over Tens of Seconds. *Chem Sci* **2018**, *9* (38), 7546–7555. https://doi.org/10.1039/c8sc02348d.

(37) Lei, R.; Tang, Y.; Yan, S.; Qiu, W.; Guo, Z.; Tian, X.; Wang, Q.; Zhang, K.; Ju, S.; Yang, S.; Wang, X. De-Pinning Fermi Level and Accelerating Surface Kinetics with an ALD Finish Boost the Fill Factor of BiVO4 Photoanodes to 44%. *Small* **2024**, *20* (7), 2306513. https://doi.org/https://doi.org/10.1002/smll.202306513.

(38) Shi, Q.; Murcia-López, S.; Tang, P.; Flox, C.; R. Morante, J.; Bian, Z.; Wang, H.; Andreu, T. Role of Tungsten Doping on the Surface States in BiVO4 Photoanodes for Water Oxidation: Tuning the Electron Trapping Process. *ACS Catal* **2018**, *8* (4), 3331–3342. https://doi.org/10.1021/acscatal.7b04277.

(39) Hu, J.; Zhao, X.; Chen, W.; Su, H.; Chen, Z. Theoretical Insight into the Mechanism of Photoelectrochemical Oxygen Evolution Reaction on BiVO4 Anode with Oxygen Vacancy. *The Journal of Physical Chemistry C* **2017**, *121* (34), 18702–18709. https://doi.org/10.1021/acs.jpcc.7b05884.

(40) Yalavarthi, R.; Zbořil, R.; Schmuki, P.; Naldoni, A.; Kment, S. Elucidating the Role of Surface States of BiVO 4 with Mo Doping and a CoOOH Co-Catalyst for Photoelectrochemical Water Splitting. *J Power Sources* **2021**, *483*, 229080. https://doi.org/10.1016/j.jpowsour.2020.229080.

(41) Tang, J.; Durrant, J. R.; Klug, D. R. Mechanism of Photocatalytic Water Splitting in TiO2. Reaction of Water with Photoholes, Importance of Charge Carrier Dynamics, and Evidence for Four-Hole Chemistry. *J Am Chem Soc* **2008**, *130* (42), 13885–13891. https://doi.org/10.1021/JA8034637.

(42) Cowan, A. J.; Tang, J.; Leng, W.; Durrant, J. R.; Klug, D. R. Water Splitting by Nanocrystalline TiO 2 in a Complete Photoelectrochemical Cell Exhibits Efficiencies Limited by Charge Recombination. *Journal of Physical Chemistry C* **2010**, *114* (9), 4208–4214. https://doi.org/10.1021/JP909993W.

(43) Kanan, M. W.; Yano, J.; Surendranath, Y.; Dincă, M.; Yachandra, V. K.; Nocera, D. G. Structure and Valency of a Cobalt−Phosphate Water Oxidation Catalyst Determined by in Situ X-Ray Spectroscopy. *J Am Chem Soc* **2010**, *132* (39), 13692–13701. https://doi.org/10.1021/ja1023767.

(44) Cao, D.; Liu, D.; Chen, S.; Moses, O. A.; Chen, X.; Xu, W.; Wu, C.; Zheng, L.; Chu, S.; Jiang, H.; Wang, C.; Ge, B.; Wu, X.; Zhang, J.; Song, L. Operando X-Ray Spectroscopy Visualizing the Chameleon-like Structural Reconstruction on an Oxygen Evolution Electrocatalyst. *Energy Environ Sci* **2021**, *14* (2), 906–915. https://doi.org/10.1039/d0ee02276d.